AGARD

ADVISORY GROUP FOR AEROSPACE RESEARCH & DEVELOPMENT

7 RUE ANCELLE 92200 NEUILLY SUR SEINE FRANCE

Paper Reprinted from
AGARDograph No. 251

THEORY AND APPLICATIONS OF OPTIMAL CONTROL IN AEROSPACE SYSTEMS

Ed by Pieter Kant
July 1981

NORTH ATLANTIC TREATY ORGANIZATION

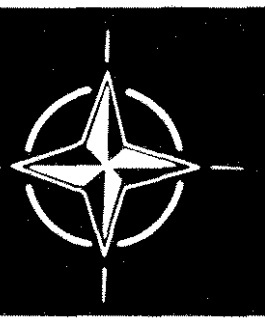

OPTIMUM CLIMB AND DESCENT TRAJECTORIES FOR AIRLINE MISSIONS

Heinz Erzberger
Research Scientist
Ames Research Center, NASA, Moffett Field, California 94035

SUMMARY

The characteristics of optimum fixed-range trajectories whose structure is constrained to climb, steady cruise, and descent segments are derived by application of optimal control theory. The performance function consists of the sum of fuel and time costs, referred to as direct operating cost (DOC). The state variable is range to go and the independent variable is energy. In this formulation a cruise segment always occurs at the optimum cruise energy for sufficiently large range. At short ranges (400 n. mi. and less), a cruise segment may also occur below the optimum cruise energy. The existence of such a cruise segment depends primarily on the fuel flow vs thrust characteristics and on thrust constraints. If thrust is a free control variable along with airspeed, it is shown that such cruise segments will not generally occur. If thrust is constrained to some maximum value in climb and to some minimum in descent, such cruise segments generally will occur. The algorithm has been implemented in a computer program that can be incorporated in an airline flight planning system or can serve as a basis for an onboard implementation. The various features of the program are described and the characteristics of the optimum trajectories are illustrated with a set of example trajectories for an aircraft model representative of the Boeing 727-100.

NOMENCLATURE

c_f	fuel cost factor, dollars/kg (dollars/lb)
c_t	time cost factor, dollars/hr
D	drag force
D_V, D_{V^2}	first and second partial derivatives of drag with respect to airspeed
d_c	cruise distance
d_f	desired distance to fly
d_{up}, d_{dn}	total climb and descent distances, respectively
E	total aircraft energy in units of altitude
E_c	cruise or maximum energy
$E_{c_{opt}}$	optimum cruise energy
E_i, E_f	initial and final energy
$\dot{E}$	rate of change in energy
g	acceleration of gravity
H	Hamiltonian, dollars per unit of energy
h	altitude, m (ft)
I_{up}, I_{dn}	components of the Hamiltonian
J	value of performance function, dollars/kg (dollars/lb)
KIAS	indicated airspeed, knots
K_{up}, K_{dn}	operands under the minimization operator in H
K_1	constant in climb fuel relation
L	lift force
P	integrand of cost function or cost per unit time
S_{FC}	thrust specific fuel consumption per hr
$S_{FC_{(\cdot)^n}}$	nth partial derivatives of S_{FC} with respect to $(\cdot)$
T	thrust, kg (lb)
T_{up}, T_{dn}	climb and descent thrusts, respectively
t	time
t_c	time at end of climb
t_d	time at start of descent
t_f	total mission time
V	true airspeed
V_c	cruise speed
V_{up}, V_{dn}	climb and descent airspeeds
V_w	wind speed along flightpath
$V_{w_{up}}, V_{w_{dn}}$	wind speeds in climb and descent segments, respectively, functions of altitude
W	aircraft weight in kg (lb)
W_f	total mission fuel, kg (lb)
W_i	initial aircraft weight, kg (lb)
W_{ref}	reference weight in climb fuel relation
$\dot{W}_f$	fuel flow rate, kg/hr (lb/hr)
x	distance flown, n. mi.
x_{up}, x_{dn}	climb and descent distances, running variables
β	parameter defining direction of control perturbations
γ	flightpath angle, radian
γ_{up}, γ_{dn}	climb and descent flightpath angles, respectively, radian
ΔR	length of control perturbation
$\Delta T, \Delta V$	thrust and speed perturbations relative to cruise conditions
$\lambda(E_c)$	cruise cost at cruise energy E_c, dollars/n. mi.

Index categories: Flight Operations; Guidance and Control; Navigation; Communication; Traffic Control.

π	throttle setting	λ	cruise cost per unit distance
π_{up}, π_{dn}	throttle settings in climb and descent, respectively	λ_{opt}	optimum cruise cost over all energies, per unit distance
ψ	costate variable		

INTRODUCTION

The continuing rise in airline operating costs due to escalating fuel prices and other inflationary factors has stimulated interest in techniques for trajectory optimization. Recent work has focused on the derivation of simplified algorithms for computing trajectories with specified range. Such an algorithm was described in Ref. 1. The trajectories calculated by this algorithm, unlike those obtained by classical performance optimization, minimize an integral performance measure such as total mission fuel cost.

Another problem that has received attention recently concerns the optimality of steady-state cruise flight. Steady-state cruise is generally not optimum for minimum fuel performance (Ref. 2), but the performance penalty of steady-state cruise is unknown because the actual nonsteady or cyclic optimum cruise has not been computed to date. However, if the steady-state cruise satisfies first-order necessary conditions, Speyer (Ref. 2) shows, in an example, that the performance improvement of a particular (though nonoptimum) cyclic cruise is about 0.1%. This improvement, if representative of the optimum cyclic cruise, is not economically significant. Nevertheless, the determination of the optimum cyclic cruise poses an interesting and unsolved problem.

Even if economically significant, cyclic cruise could not be used in airline operation because it is incompatible with existing air traffic control procedures, disconcerts passengers, and decreases engine life. Optimum trajectories, to be compatible with typical airline practice, should consist of a climbout, a steady-state cruise, and a descent. Thus, at least for commercial airline applications, the optimum trajectory must be selected from a set of trajectories that is limited *a priori* to such types.

A formulation of the trajectory optimization problem that constrains the admissible trajectories to those containing climb, steady cruise, and descent was given in Ref. 1. In this formulation, energy height was used as the independent or timelike variable in climb and descent, thus forcing energy to change monotonically in these segments. It was shown that the use of energy as the independent variable eliminates the integration of a separate adjoint differential equation, thus simplifying the numerical solution of the optimal control problem. Therefore, this formulation is also adopted here.

An evaluation of the constrained optimum trajectories by airline operators indicated an interest in the additional constraint of setting the thrust to some maximum during climb and to idle during descent to reduce pilot workload of flying the trajectories. An examination of this procedure raised the following questions that are investigated here. How do the constraints on thrust and, more generally, the aerodynamic and propulsion characteristics affect the structure of the trajectories? Under what condition is the constrained thrust procedure optimum? What performance penalty is incurred by the constraint on thrust?

The avionics and aircraft industry is currently developing onboard performance computer systems to assist the flight crew in minimizing fuel consumption and operating costs. Because of its modest computational requirements, the algorithm described herein can be implemented in an onboard computer. This paper briefly describes a computer implementation of the algorithm and also discusses the characteristics of several optimum trajectories computed for the Boeing 727-100 aircraft.

OPTIMAL CONTROL FORMULATION

As stated in the Introduction, we assume at the outset that the optimum trajectories have the structure shown in Fig. 1. This structure consists of climb, cruise, and descent segments, with the aircraft energy increasing monotonically in climb and decreasing monotonically in descent. Neglecting flightpath-angle dynamics and weight loss due to fuel burn, the point mass equations of motion for flight in the vertical plane are

$$(1/g)(dV/dt) = [(T - D)/W] - \sin\gamma \tag{1}$$

$$dh/dt = V \sin\gamma \tag{2}$$

$$dx/dt = V \cos\gamma + V_W \approx V + V_W \tag{3}$$

with the constraint $L = W \cos\gamma$. The along-track wind component V_W may be a function of altitude, but accelerations due to wind shears as well as the vertical wind component can be neglected in this analysis. In airplanes, unlike rockets, the rate of change of weight due to fuel burn introduces negligible dynamic effects in the trajectory optimization. Nevertheless, the effect of weight loss on a trajectory is important but can be accounted for without adding another state variable by techniques described in the section on computer implementation. If energy is defined as

$$E = h + (1/2g)V^2 \tag{4}$$

then the familiar relation for the rate of change in energy is obtained by differentiating Eq. (4) with respect to time and substituting the right-hand sides of Eqs. (1) and (2) in place of dV/dt and dh/dt, respectively:

$$\dot{E} \equiv dE/dt = [(T - d)V]/W \tag{5}$$

The cost function to be minimized is chosen as the direct operating cost of the mission and consists of the sum of the fuel cost and the time cost:

$$J = c_f W_f + c_t t_f \tag{6}$$

where c_f and c_t are the unit costs of fuel and time, respectively. Setting $c_t = 0$ results in the familiar minimum fuel performance function. In integral form, the cost function becomes

$$J = \int_0^{t_f} (\dot{W}_f c_f + c_t)dt \equiv \int_0^{t_f} P\ dt \tag{7}$$

It is assumed that the time to fly, t_f, is a free variable, but the distance to fly is a specified quantity d_f. Following the formulation in Ref. 1, we now write the total mission cost as the sum of the costs for the three segments of the assumed trajectory (illustrated in Fig. 1);

$$J = \underbrace{\int_0^{t_c} P\ dt}_{\substack{\text{climb}\\ \text{cost}}} + \underbrace{(d_f - d_{up} - d_{dn})\lambda}_{\substack{\text{cruise}\\ \text{cost}}} + \underbrace{\int_{t_d}^{t_f} P\ dt}_{\substack{\text{descent}\\ \text{cost}}} \tag{8}$$

where λ designates the cost of cruising at a given energy E_c. Next, we transform the integral cost terms in Eq. (8) by changing the independent variable from time to energy, using the transformation $dt = dE/\dot{E}$:

$$J = \int_{E_i}^{E_c} (P/\dot{E}\big|_{\dot{E}>0})dE + (d_f - d_{up} - d_{dn})\lambda + \int_{E_f}^{E_c} (P/|\dot{E}|_{\dot{E}<0})dE \tag{9}$$

where E_i and E_f are the given initial climb and final descent energies, respectively. The transformation uses the assumption that the energy changes monotonically in climb and descent. This places strict inequality constraints on $\dot{E}$, as shown in Eq. (9). Also in Eq. (9), the integration limits have been reversed in the descent cost term. In this formulation the cost function is of mixed form, containing two integral cost terms and a terminal cost term contributed by the cruise segment.

With the change in independent variable from time to energy, the state equation (Eq. (5)) is eliminated, leaving Eq. (3) as the only state equation. Furthermore, we note that the performance function (Eq. (9)) depends on the distance state x only through the sum of the climb and descent distances $d_{up} + d_{dn}$. Therefore, the state equation for the distance is rewritten in terms of this sum as:

$$d(x_{up} + x_{dn})/dE = \left(V_{up} + V_{w_{up}}\right)\Big/\dot{E}\big|_{\dot{E}>0} + \left(V_{dn} + V_{w_{dn}}\right)\Big/|\dot{E}|_{\dot{E}<0} \tag{10}$$

Here the transformation $dt = dE/\dot{E}$ was used again. Also, Eq. (10) provides for independence in the choice of climb and descent speeds V_{up} and V_{dn} and the wind velocities $V_{w_{up}}$ and $V_{w_{dn}}$. Wind velocities in climb and descent are allowed to be independent of each other; generally, different wind conditions will prevail in physically different locations of climb and descent. The wind velocities can also be altitude-dependent. The effect of altitude-dependent winds on the optimum trajectories is discussed in Ref. 3.

Necessary conditions for the minimization of Eq. (9), subject to the state equation (Eq. (10)) are obtained by application of optimum control theory (see, e.g., Ref. 4, p. 71). Then the following relations are obtained for the Hamiltonian and costate equations, respectively:

$$H = \min_{\substack{V_{up},V_{dn}\\ \pi_{up},\pi_{dn}}} \left\{ \left(\frac{P}{\dot{E}}\right)_{\dot{E}>0} + \left(\frac{P}{|\dot{E}|}\right)_{\dot{E}<0} + \psi\left[\frac{V_{up} + V_{w_{up}}}{\dot{E}\big|_{\dot{E}>0}} + \frac{V_{dn} + V_{w_{dn}}}{|\dot{E}|_{\dot{E}<0}}\right] \right\} \tag{11}$$

$$d\psi/dE = -[\partial H/\partial(x_{up} + x_{dn})] = 0 \tag{12}$$

The right-hand side of the Hamiltonian equation is minimized with respect to two pairs of control variables, one pair applicable to climb (V_{up} and π_{up}), the other pair to descent (V_{dn} and π_{dn}). Since each term under the minimization operator in Eq. (11) contains only one of the two pairs of control variables, the minimization simplifies into two independent minimizations, one involving climb controls, the other, descent controls. Also, since the right-hand side of the costate equation (Eq. (12)) is zero, ψ is constant.

TRANSVERSALITY CONDITIONS

The transversality conditions are additional necessary conditions that depend on the end-point constraints of state variables (Ref. 4). The basic constraint in this problem is that the range of the trajectory be d_f. However, d_f is a parameter in the transformed cost function, Eq. (9), and not a state variable. The final value of the state variable $d_{up} + d_{dn}$ is, in this formulation, subject only to the inequality constraint $d_{up} + d_{dn} \leq d_f$. This constraint is, of course, necessary for a physically meaningful result. This inequality constraint can be handled by solving two optimization problems, one completely free ($d_{up} + d_{dn} < d_f$), the other constrained ($d_{up} + d_{dn} = df$), and then choosing the trajectory with the lowest cost. Physically, the comparison is between a trajectory with a cruise segment and one without a cruise segment. Considering first the free terminal state case, $d_{up} + d_{dn} < d_f$, we obtain the following relation for the final value of the costate ψ:

$$\psi(E_c) = \left.\frac{\partial(d_f - x_{up} - x_{dn})\lambda}{\partial(x_{up} + x_{dn})}\right|_{E=E_c, x_{up}=d_{up}, x_{dn}=d_{dn}} = -\lambda \qquad (13)$$

This is the transversality condition for the free final state problem with terminal cost (Ref. 4). It shows that the constant costate value is the negative of the cruise cost.

Next, consider the case of no cruise segment. Then, the middle term of Eq. (9) drops out and the performance function contains only the integral cost terms. This is the case of the specified final state $d_f = d_{up} + d_{dn}$; the corresponding transversality condition yields $\psi(E_c) = \psi_f$. In practice it is not necessary to compute the constrained terminal state trajectory if a valid free terminal state trajectory exists, i.e., one for which $d_f > d_{up} + d_{dn}$, since the addition of a terminal constraint can only increase the cost of the trajectory. Therefore, this case is not considered further here.

In both cases the choice of costate determines a particular range. Since the functional relationship between these variables cannot be determined in closed form, it is necessary to iterate on the costate value to achieve a specified range d_f.

The last necessary condition applicable to this formulation is obtained by making use of the fact that the final value of the timelike independent variable E is free. Its final value is the upper limit of integration E_c in Eq. (9). Application of results in Ref. 4 provides the following condition:

$$\left(H + \left\{\partial[(d_f - d_{up} - d_{dn})\lambda(E)]/\partial E\right\}\right)_{E=E_c} = 0 \qquad (14)$$

which, when evaluated and simplified, becomes

$$\left\{H + [d_c(d\lambda/dE)]\right\}_{E=E_c} = 0 \qquad (15)$$

where d_c is the cruise distance.

Condition (15) has the following physical interpretation. The value of the Hamiltonian H evaluated at cruise energy E_c is (after substituting Eq. (13) into (11)) the minimum increment in the sum of climb cost and descent cost to make a unit increment in cruise energy. The product $d_c(d\lambda/dE)_{E=E_c}$ is the increment in cruise cost resulting from a unit change in cruise energy. Condition (15) requires the optimum trajectory to be such that the sum of these two increments be zero for a given cruise distance d_c and cruise energy E_c.

DEPENDENCE OF OPTIMUM TRAJECTORIES ON RANGE

Equation (15), together with knowledge of the salient characteristics of the cruise cost λ and the Hamiltonian H, can be used to determine the structural dependence of the optimum trajectories on range.

Cruise cost at a cruise energy E_c and cruise speed V_c is computed from the relation

$$\lambda(E_c, V_c) = [P(T, E_c, V_c)]/(V_c + V_w) \quad \text{with constraints} \quad \begin{cases} T = D \\ L = W \end{cases} \qquad (16)$$

where the denominator is the ground speed in the flightpath direction. Examination of the term containing λ in the relation for the performance function (9) shows that the value for λ should be as small as possible at each cruise energy to minimize the total cost J. Therefore, the cruise-speed dependence of λ is eliminated by minimizing the right side of Eq. (16) with respect to V_c:

$$\lambda(E_c) = \min_{V_c} P(T, E_c, V_c)/(V_c + V_w) \qquad (17)$$

In this paper, λ and V_c are always assumed to be the optimum cruise cost and cruise speed, respectively, at a particular cruise energy E_c.

Except in high wind shear, the cruise cost as a function of cruise energy exhibits the roughly parabolic shape shown in Fig. 2. For subsonic transport aircraft, the minimum of the cruise cost with respect to energy occurs close to the maximum energy boundary. This characteristic of the cruise cost prevails for essentially all values of the performance function parameters c_f and c_t. The quantities defining the optimum cruise conditions are $E_{c_{opt}}$ and λ_{opt}. In Eq. (15), the derivative of the cruise cost function multiplies the cruise distance. Except under extreme wind shear conditions, the derivative is monotonic and crosses the zero axis at $E_c = E_{c_{opt}}$.

By distributing the minimization operator in Eq. (11) and substituting Eq. (13) in Eq. (11), H can be decomposed into climb and descent components as follows:

$$H[E, \lambda(E_c)] = I_{up} + I_{dn} \qquad (18)$$

where

$$I_{up} = \min_{\substack{V_{up} \\ \pi_{up}}} \left[\frac{P - \lambda(V_{up} + V_{w_{up}})}{\dot{E}\big|_{\dot{E}>0}}\right], \qquad I_{dn} = \min_{\substack{V_{dn} \\ \pi_{dn}}} \left[\frac{P - \lambda(V_{dn} + V_{w_{dn}})}{|\dot{E}|_{\dot{E}<0}}\right] \qquad (19)$$

In the preceding section, the Hamiltonian, evaluated at $E = E_c$, was interpreted as the cost penalty to achieve a unit increase in cruise energy. Extensive numerical studies of Eq. (18) for several comprehensive models of subsonic turbofan aircraft show $H[E_c,\lambda(E_c)] \geq 0$ for $E_c \leq E_{c_{opt}}$. Moreover, the minimum cost penalty for increasing energy I_{up} is always positive and that for decreasing I_{dn} is negative, but the sum has never been found negative for models of currently used turbofans. While these characteristics have been established for several aircraft models, they are not intended to imply a generalization to all aircraft since no physical laws prevent H from being negative.

Consider first the case where $H[E_c,\lambda(E_c)] > 0$. Then Eq. (15) can be solved for the cruise distance d_c:

$$d_c = -H[E_c,\lambda(E_c)]/(d\lambda/dE)_{E=E_c} \tag{20}$$

Since $d\lambda/dE < 0$, but approaches zero as $E_c \to E_{c_{opt}}$, the cruise distance must increase without limit as $E_c \to E_{c_{opt}}$. Our numerical studies have shown that the value of H tends to decrease as E_c increases, but not enough to change this trend. Figure 3 shows the resulting family of trajectories, assuming $H > 0$ for all values of E_c. In this case, interestingly, nonzero cruise segments occur at short ranges and at energies below the optimum cruise energy $E_{c_{opt}}$. Optimum cruise is approached asymptotically at long range.

Consider next the case where $H[E_c,\lambda(E_c)] = 0$. Then $d_c = 0$, i.e., no cruise segment is present for $d\lambda/dE < 0$. However, Eq. (15) shows that d_c can be nonzero $d\lambda/dE = 0$. This implies that, for $H = 0$, cruise flight is optimum only at the optimum cruise energy $E_{c_{opt}}$. Figure 4 shows the family of trajectories for this case.

THRUST OPTIMIZATION FOR MINIMUM FUEL TRAJECTORIES

Evaluation of the Hamiltonian equation would be simplified if one of the two pairs of control variables, airspeed or thrust, could somehow be eliminated *a priori* from the minimization. Since the pair of throttle settings, π_{up} and π_{dn}, is thought to be near its limit, we shall look for conditions where extreme settings of the throttle are optimum. The remainder of this paper examines only the minimum fuel case $c_f = 1$ and $c_t = 0$, with winds set to zero to simplify the derivation. However, the results can be extended to the more general cost function.

For minimum fuel performance, the two terms in the Hamiltonian Eq. (19) become

$$I_{up} = \min_{\pi_{up},V_{up}} K_{up} \quad , \quad I_{dn} = \min_{\pi_{dn},V_{dn}} K_{dn} \tag{21a}$$

where

$$K_{up} \equiv \left[\frac{\dot{W}_f - \lambda V_{up}}{(T - D)V_{up}/W}\right]_{T(\pi_{up})>D} \quad ; \quad K_{dn} \equiv \left[\frac{\dot{W}_f - \lambda V_{dn}}{|T - D|V_{dn}/W}\right]_{T(\pi_{dn})<D} \tag{21b}$$

An accurate model for thrust and fuel flow generally includes the functional dependencies, $T(\pi,V,h)$ and $\dot{W}_f(\pi,V,h)$. In addition, these functions must be corrected for nonstandard temperatures and bleed losses.

In previous work on aircraft trajectory optimization (Ref. 5), a simpler model for fuel flow and thrust was used:

$$\dot{W}_f = TS_{FC}(V,h) \quad ; \quad T_{min}(V,h) \leq T \leq T_{max}(V,h) \tag{22}$$

The critical assumption in Eq. (22) is independence of the specific fuel consumption S_{FC} from thrust. The virtue of this model lies in the insight it yields into the minimum fuel problem. If Eq. (22) is substituted into Eqs. (21b), one obtains

$$K_{up} = \frac{S_{FC}W}{V_{up}}\left[\frac{T_{up} - (\lambda/S_{FC})V_{up}}{T_{up} - D}\right]_{T_{up}>D} \quad ; \quad K_{dn} = \frac{S_{FC}W}{V_{dn}}\left[\frac{T_{dn} - (\lambda/S_{FC})V_{dn}}{|T_{dn} - D|}\right]_{T_{dn}<D} \tag{23}$$

For any fixed values of V_{up} or V_{dn}, the operand functions for the minimization of K_{up} and K_{dn} are hyperbolas with poles at $T = D$. The numerator zero must be to the left of the pole on the thrust axis for energies less than cruise energy. Figure 5 is a typical plot of these functions. Clearly, maximum thrust minimizes K_{up} and idle thrust minimizes K_{dn} for any $E < E_c$, proving that the limiting values of thrust are optimum for this propulsion model throughout the climb and descent trajectories. This result also implies that the departure from the extreme thrust values found for the more general propulsion model is directly attributable to the nonlinear dependence of fuel flow on thrust. Conversely, the need for throttle setting optimization can be determined *a priori* from the fuel flow vs thrust dependence for a particular engine. Such data are found in the engine manufacturer's performance handbook.

EVALUATION OF HAMILTONIAN AT CRUISE

We have seen in a preceding section that the value of the Hamiltonian computed at cruise energy E_c determines the structure of the trajectories near cruise. Here we shall relate the existence of cruise below $E_{c_{opt}}$ to specific engine and aerodynamic model parameters by substituting truncated Taylor series expansions of fuel flow and drag as functions of airspeed and thrust into the expression for the Hamiltonian. The location of the minimum with respect to the controls as well as the value of H can then be determined as functions of the Taylor series coefficients at $E = E_c$.

How should one pick the point in the control space about which to make the expansion? Computational experience in Refs. 1 and 3 has shown that the minimum is in the neighborhood of the optimum cruise speed and throttle setting, corresponding to the given cruise energy. This suggests that the cruise controls should be picked for the expansion point.

The fuel flow and drag functions expanded to second order about the cruise controls $T = T_c$, $V = V_c$ are

$$\dot{W}_f = T_c S_{FC} + \left(T_c S_{FC_T} + S_{FC}\right)\Delta T + T_c S_{FC_V}\,\Delta V + (1/2)\left(2S_{FC_T} + T_c S_{FC_{T^2}}\right)\Delta T^2$$
$$+ \left(T_c S_{FC_{TV}} + S_{FC_V}\right)\Delta V\,\Delta T + (1/2) T_c S_{FC_{V^2}}\,\Delta V^2 + \text{higher-order terms} \tag{24}$$

$$D = D(V_c, E_c) + D_V\,\Delta V + (1/2) D_{V^2}\,\Delta V^2 + \text{higher-order terms} \tag{25}$$

The subscripts to S_{FC} and D designate the partial derivatives with respect to the subscripted variable. Note that the expansion allows for a general fuel flow model in which specific fuel consumption can be thrust-dependent.

Before substituting Eqs. (24) and (25) into the expression for H, we observe that H is singular at cruise with $T = T_c$ and $V = V_c$, because both numerator and denominator are identically zero at that point. Figure 6 plots the loci of the numerator and denominator zeros of K_{up} and K_{dn} in the control space at $E = E_c$. It is proved in the Appendix that the locus of numerator zeros is tangent to the locus of denominator zeros at the optimum cruise controls. For $E < E_c$, the two loci have no points in common. The two loci can be tangent but cannot cross since, otherwise, controls would exist that would make the Hamiltonian infinitely negative, a result ruled out as physically meaningless.

Upon substituting Eqs. (24) and (25) into (21) using the tangency condition (A4) derived in the Appendix, the following expressions for K_{up} and K_{dn} at cruise energy are obtained:

$$\left.\begin{matrix} K_{up} \\ \text{or} \\ K_{dn} \end{matrix}\right\} = \frac{W}{(V_c + \Delta V)} \left\{ \frac{\left[\begin{matrix} \left(T_c S_{FC_T} + S_{FC}\right)\Delta T - \left(D_V S_{FC} + T_c S_{FC_T} D_V\right)\Delta V \\ + (1/2)\left(2S_{FC_T} + T_c S_{FC_{T^2}}\right)\Delta T^2 + \left(T_c S_{FC_{TV}} + S_{FC_V}\right)\Delta V\,\Delta T \\ + (1/2) T_c S_{FC_{V^2}}\,\Delta V^2 \end{matrix}\right]}{\left|\Delta T - D_V\,\Delta V - (1/2) D_{V^2}\,\Delta V^2\right|} \right\} \tag{26}$$

Terms above second order have been neglected since we are investigating a small neighborhood of the cruise point. Expression (26) represents K_{up} if the quantity under the absolute value sign is positive and K_{dn} if it is negative.

Since the cruise point at $\Delta T = 0$ and $\Delta V = 0$ gives the undefined value of 0/0 for Eq. (26), it is necessary to evaluate the limit as ΔT and ΔV approach zero. If the limit exists, it must be independent of the direction from which the cruise point is approached. To compute the limit and investigate the neighborhood of the cruise point, a polar coordinate system centered at the cruise point is used to define control perturbations. Let ΔR and β define control perturbations ΔT and ΔV as follows:

$$\Delta T = (D_V + \beta)\Delta V \tag{27}$$

$$\Delta V = \frac{\Delta R}{\sqrt{1 + (\beta + D_V)^2}}\,, \qquad \Delta T = \frac{\Delta R(\beta + D_V)}{\sqrt{1 + (\beta + D_V)^2}} \tag{28}$$

The parameter β defines a direction relative to the reference direction of the line $\Delta T = D_V\,\Delta V$. The reference direction $\beta = 0$ is excluded from the control space since it is along the direction of the locus of $T = D$ at the cruise point.

After substituting Eqs. (28) into (26) and taking the limit of the resulting expressions as $\Delta R \to 0$, one obtains for any $\beta \neq 0$:

$$K_{up}\Big]_{\text{limit}} = (W/V_c)\left(S_{FC} + T_c S_{FC_T}\right)\,, \quad K_{dn}\Big]_{\text{limit}} = (-W/V_c)\left(S_{FC} + T_c S_{FC_T}\right) \tag{29}$$

The limit is thus well defined since it is independent of the approach direction in each region. However, it remains to be shown that the limit value is in fact the minimum of Eq. (26) with respect to the perturbation controls. This question is investigated for two cases, one for which S_{FC} is independent, and the other, dependent on thrust.

Case (A): S_{FC} Independent of Thrust

Along the direction defined by $\Delta V = 0$, i.e., along the thrust direction, Eq. (23) can be used directly to determine the dependence of the functions on T_{up} and T_{dn} under the minimization operator. Since at $V = V_c$, $D(V_c,E_c) = T_c = (\lambda/S_{FC})V_c$, Eq. (23) reduces to

$$K_{up} = (W/V_c)S_{FC} \ , \quad K_{dn} = (W/V_c)S_{FC} \tag{30}$$

showing that, at the cruise speed V_c, these functions are independent of thrust. This result is not restricted to small perturbations relative to the cruise thrust. Along other directions, the truncated Taylor series form (Eq. (26)) must be used. After setting the zero all thrust-dependent derivatives and substituting Eqs. (28) into (26), the following expression is obtained.

$$\begin{matrix} K_{up} \\ \text{or} \\ K_{dn} \end{matrix} = \frac{WS_{FC}}{(V_c + \Delta V)} \left[\frac{\pm 1 + \dfrac{\left(2S_{FC_V}(|\beta| + D_v) + T_c S_{FC_{V^2}}\right)\Delta R}{2|\beta| S_{FC} \sqrt{1 + (\beta + D_v)^2}}}{\left| 1 - \dfrac{D_{v^2}\, \Delta R}{2|\beta| \sqrt{1 + (\beta + D_v)^2}} \right|} \right] \tag{31}$$

where the positive sign applies to K_{up} and the negative sign to K_{dn}. The characteristics of these functions depend on the drag and specific fuel consumption derivatives. The drag derivatives D_V and D_{V^2} are both positive since the aircraft will certainly operate on the "front" side of the thrust-required curve. The dependence of S_{FC} on speed for a typical, currently in-service turbofan engine at cruise energies exhibits a slight upward curvature above Mach 0.4 (as shown in Fig. 7), implying that both S_{FC_V} and $S_{FC_{V^2}}$ are positive in the range of interest between Mach 0.4 and 0.9. The slight curvature of S_{FC} indicates that a quadratic function can accurately model the Mach number dependence of S_{FC} in the Mach range of interest and not just in a small neighborhood of the expansion point. Also, at typical cruise conditions, one finds that $D_{V^2} > (2S_{FC_V}D_V + T_c S_{FC_{V^2}})$. Therefore, for any β, the denominator of Eq. (31) goes to zero before the numerator does as ΔR is increased from an initial value of zero. Moreover, the slope of the operand function with respect to ΔR increases as $\beta \to 0$. The effect of ΔV can be neglected since $V_c >> \Delta V$.

These observations lead to the conclusion that the functions in Eq. (31) slope upward in all directions as ΔR increases, except in the direction parallel to the thrust axis, along which the slope is level. Figure 8 shows a family of plots of the operand functions as β varies over its range. The limiting values of these functions at the cruise point $(\pm W/V_c)S_{FC}$ are therefore also the global minimums, and the value of the Hamiltonian, which is the sum of the two components, is zero. At the cruise energy, furthermore, the optimum climb and descent speeds are equal to the optimum cruise speed. The optimum climb and descent thrusts at that point are arbitrary since the Hamiltonian is independent of them.

By applying these results to Eq. (20), it now follows that the structure of the optimum trajectories near cruise is given by the family of trajectories in Fig. 4. Specifically, no cruise segment occurs except at optimum cruise energy $E_{c_{opt}}$.

By combining results from this and the preceding section, the important result follows that, for the assumed engine model, optimum trajectories, corresponding optimum controls, and performance are not affected by constraining the thrust to extreme values in the climb and descent segments.

Case (B): S_{FC} Thrust-Dependent

A complete investigation of the neighborhood of the cruise point analogous to Case (A) requires estimates of the various thrust-dependent derivatives in Eq. (26). However, understanding of this case can be obtained by examining the functions in Eq. (26) only along the thrust direction, i.e., for $\Delta V = 0$. Under that assumption, Eq. (26) simplifies to:

$$\begin{matrix} K_{up} \\ \text{or} \\ K_{dn} \end{matrix} = (WS_{FC}/V_c \left[\pm 1 + \left(T_c S_{FC_T}/S_{FC}\right) + (|\Delta T|/2S_{FC})\left(2S_{FC_T} + T_c S_{FC_{T^2}}\right) \right] \tag{32}$$

where the plus sign and $\Delta T > 0$ are chosen for K_{up} and the negative sign and $\Delta T < 0$ for K_{dn}.

This simplified approach focuses attention on the derivatives S_{FC_T} and $S_{FC_{T^2}}$, which are crucial for this case. The characteristics of these derivatives can be deduced from plots of S_{FC} vs thrust (Fig. 9). These plots, and those in Fig. 7, were derived from the operating instructions manual of a typical in-service turbofan (Ref. 6). Obviously, the assumption of a thrust-independent S_{FC} is grossly violated for this engine since, at low thrust values, the S_{FC} curves approach infinity; i.e., they become undefined. However, at typical climb or cruise thrusts, corresponding to the upper half of the thrust range, the variation in S_{FC} is only about 5%.

Fuel flow is also plotted in Fig. 9. The dashed line through the origin gives the best constant SFC approximation to the fuel flow function. Comparison indicates an excellent match at high thrust, but an error of as much as 1200 lb/hr (550 kg/hr) at low thrust. For some applications the assumption of a constant S_{FC} could be adequate if fuel flow errors at very low or idle thrust settings can be tolerated.

For the upper two thirds of the thrust range, quadratic functions provide good fits to the S_{FC} curves. Therefore, one can use the second-order Taylor series expansion at the cruise point to estimate S_{FC} for fairly large deviations of thrust from cruise thrust.

The thrust in climb or cruise is typically larger than the thrust at which S_{FC} is a minimum in Fig. 9. Both S_{FC_T} and $S_{FC_{T2}}$ will therefore be greater than zero and so will the coefficient of ΔT in Eq. (32). It follows that the slope of Eq. (32) as a function of Δt is greater than zero for K_{up} and less than zero for K_{dn}. In other words, along the thrust direction these functions have a strong minimum at the cruise point whereas in Case (A) they were level along this direction. Along other directions, the investigation of Case (A) has shown a positive slope. Thus, if thrust is an unconstrained control variable along with airspeed, so that the cruise point lies in the interior of the control region, then the optimum climb and descent thrusts and airspeeds will converge toward the optimum cruise thrust and airspeed as the climb and descent energies approach the cruise energy. It should be noted that this holds for all cruise energies, including those less than the optimum cruise energy, $E_{c_{opt}}$. Since the Hamiltonian is again zero at the cruise energy, it follows that the structure of the optimum trajectories as a function of range is identical to that of Case (A) and is illustrated by Fig. 4. Computer calculations for this case in Ref. 1, using a similar engine model, showed that the thrust is either maximum or idle for about three-fourths of the energy range between initial and cruise energies and then departs from the extremum values so as to converge smoothly to the value at cruise as cruise energy is approached.

Consider now the case where thrust is constrained to some maximum in climb and is idle in descent. In that case, the minimum at the cruise point is not accessible since it does not lie in the region of permissible controls. Also, unlike Case (A), the thrust dependence of K_{up} and K_{dn} in Eq. (23) does not disappear along the thrust direction at $V = V_c$. Therefore, it is unlikely that at the minimum the sum of the two terms will be zero. The Hamiltonian is, in fact, greater than zero at any cruise energy. In order to show this, note in Fig. 9 that, as thrust decreases, S_{FC} increases without bound. It follows that I_{dn} will be less negative than it would be if S_{FC} were thrust-independent and therefore will be insufficient to cancel I_{up} at cruise energy, resulting in a positive value for the Hamiltonian. This was shown earlier to give rise to nonzero cruise segments below the optimum cruise energy. Thus, the structure of the optimum trajectories for the constrained thrust case is given by the family of trajectories in Fig. 3.

COMPUTER IMPLEMENTATION

(a) Algorithm Description

The climb and descent profiles are generated by integrating the state equation (10) from the initial energy E_i to the maximum or cruise energy E_c. For this purpose, Eq. (10) is separated into its climb and descent components, which are then modified to include the effect of nonzero flightpath angles as follows:

$$\left.\begin{aligned} dx_{up}/dE &= \left(V_{up} + V_{w_{up}}\right)\cos\gamma_{up}/\dot{E} \\ dx_{dn}/dE &= \left(V_{dn} + V_{w_{dn}}\right)\cos\gamma_{dn}/|\dot{E}| \end{aligned}\right\} \tag{33}$$

Flightpath angles are not defined within the reduced dynamics of the energy state model. Nevertheless, during the integration of the trajectory, the flightpath angles for climb and descent, γ_{up} and γ_{dn}, can be computed by using increments of altitude and distance from two successive energy points. The use of these computed flightpath angles in Eq. (33) slightly increases the accuracy of the climb and descent distance integrations.

At each energy in the integration the optimum airspeeds and thrust settings are obtained as the values that minimize the two components of the Hamiltonian in Eq. (19). The minimization of the Hamiltonian is carried out by the Fibonacci search technique (Ref. 7). It has the advantage of using the least number of function evaluations of all known search techniques to locate the minimum with prescribed accuracy and also is well suited to handle tabular data. Fibonacci search is basically a one-variable minimization procedure. It is adapted here to two variables by applying the technique to one variable at a time while holding the other variable fixed. Convergence to the minimum is achieved by cycling between the two variable several times. Prior to a search over a given control variable, the limits of the regions for K_{up} and K_{dn}, which consist of the $T = D$ locus and the dashed line with shaded border in Fig. 6, are computed to keep the search interval as small as possible.

As previously explained, the choice of λ in the Hamiltonian determines the range of the trajectory, but the exact functional dependence between λ and range cannot be determined explicitly for the various weights, wind profiles, and other parameter changes encountered in real time operation. An iterative procedure is therefore used and is explained in part (b) of this section.

An important part of the algorithm involves accounting for the weight change due to fuel burn. The effect on the optimum trajectory of the change in weight was not included explicitly in the theory for reasons previously stated. Two methods are used to correct the optimum trajectories for the weight change. The first merely integrates the fuel flow and updates the weight in the calculation of $\dot{E}$ during climb and descent. This ensures that updated values of aircraft weight are used in the integration of Eqs. (33) to generate the climb and descent trajectories.

The second method modifies the value of λ used in the Hamiltonian. This modification involves using the estimated weight of the aircraft at the end of climb, i.e., at energy E_c, to compute the value of λ rather than the weight at takeoff. It is important to use the weight at E_c rather than the weight at some other energy, to compute λ because the sensitivity of the optimum controls to changes in λ increases as the aircraft energy approaches E_c. The fuel consumption for the entire climb trajectory, F_{up}, is estimated at the start of climb from the empirical relation:

$$F_{up} = K_1(E_c - E_i)W_i/W_{ref} \tag{34}$$

where K_1 is an aircraft-dependent constant and W_{ref} is a typical initial climb weight. This relation estimates the climb fuel weight to about 10% accuracy, which is adequate for this purpose. Similarly, the weight at the end of cruise, if a cruise segment is present, is used to compute λ for the descent optimization. The cruise fuel consumption, F_c, is determined from the relation:

$$F_c = \tilde{W} d_c / \tilde{V}_g \tag{35}$$

where $\tilde{W}$ is the average fuel flow rate and V_g the average ground speed during cruise. The calculation of the average quantities is described in Ref. 8.

The computer implementation includes both the free and constrained thrust cases. For the constrained thrust case, the cruise distance is computed from Eq. (20). However, because $d\lambda/dE \to 0$ as $E_c \to E_{c_{opt}}$, there is a practical limit to the use of Eq. (20), determined by the numerical accuracy of computing $d\lambda/dE$ for E_c in the neighborhood of $E_{c_{opt}}$. A practical limit for E_c is that value for which $\lambda = 1.01\lambda_{opt}$. The total range of the trajectory obtained for this value of λ is referred to as d_{max}. All trajectories requiring longer ranges than d_{max} are assumed to cruise at $E_{c_{opt}}$ and contain cruise segments of length $d_c = d_f - d_{up} - d_{dn}$, where d_{up} and d_{dn} are computed for $\lambda = 1.01\lambda_{opt}$. In the free thrust case, numerical difficulties can arise in minimizing Eq. (19) as $E_c \to E_{c_{opt}}$. The value of $1.01\lambda_{opt}$ has also been found to serve as a practical criterion for computing the longest range without a cruise segment at $E_{c_{opt}}$.

(b) Simplified Flow Chart

A computer program of the algorithm has been implemented in FORTRAN IV and is described in detail in Ref. 8. The program contains one main program and 38 subroutines. There are approximately 2400 FORTRAN instructions in the program. In this paper, the organization and major elements of the program are outlined with reference to the simplified flow chart shown in Fig. 10.

After reading aircraft lift, drag, and propulsion data, performance function parameters, and wind and temperature data, the optimum cruise speeds and costs and $d\lambda/dE$ are computed for a range of cruise energies and cruise weights using Eq. (17). Cruise weight is incremented in steps of about 5% of average gross weight. Cruise energy is incremented in 1000-ft steps from 5000 energy-feet to the maximum or ceiling energy. The results are stored in what is referred to as cruise performance tables. At each weight the cruise performance vs energy will show a dependence as in Fig. 2. The tables also contain a variety of other quantities such as fuel flow, thrust setting, Mach number, etc., that are needed to fly the trajectories. In addition, at each weight the optimum cruise energy $E_{c_{opt}}$ and the optimum cruise cost λ_{opt} are computed and stored in separate tables. Since these tables contain extensive amounts of data and are time consuming to compute, they can be permanently saved on a mass storage medium.

After reading in additional input data, two optimum trajectories referred to as the minimum and maximum range trajectories are synthesized. The minimum range trajectory is obtained by choosing the largest value of λ (called λ_{max}) stored in the cruise performance tables at the gross weight of interest. The maximum range trajectory is obtained by choosing the smallest λ, namely, $1.01\lambda_{opt}$, as explained in part (2). Values of λ at given weights are computed by interpolating between data points in the cruise tables. The corresponding ranges d_{max} and d_{min} can now be compared with d_f to decide on the type of trajectory required. If $d_f > d_{max}$, the trajectory will always contain a segment of cruise at optimum cruise energy $E_{c_{opt}}$. No iteration on λ is required in this case since the specified range d_f is obtained by choosing a cruise segment of length $d_c = d_f - d_{up} - d_{dn}$. The optimum altitude and Mach number in the cruise segment are updated every 100 n. mi. to account for the loss of weight due to fuel burn. This is the well-known climb-cruise technique.

If $d_{min} \leq d_f \leq d_{max}$, the maximum energy will fall below $E_{c_{opt}}$ and iteration with respect to λ is required. Here the approximately known inverse relationship between λ and d_f, illustrated in Fig. 11 for a Boeing 727-100, is incorporated in heuristic to minimize the iteration. Thus, the first estimate of λ is computed from

$$\lambda = (A/d_f) + B \tag{36}$$

The constants A and B are chosen to yield λ_{max} and $1.01\lambda_{opt}$ when d_f is set to d_{min} and d_{max}, respectively. Then the trajectory is synthesized to yield the actual range d. If d is not sufficiently close to d_f, constants A and B are updated by using a pair of ranges and the corresponding pair of λ's computed in preceding syntheses. The ranges included in this pair are selected so they enclose the desired range and lie closest to it. A new estimate of λ is now computed and the synthesis is repeated. Typically, after two iterations the actual range will have converged to within 5 n. mi. of the specific range and iteration is terminated.

The optimum climb and descent trajectory is specified by storing the range, time, fuel, Mach number, thrust setting, and altitude as a function of energy height in 500 energy-feet increments.

The computer implementation of the algorithm described here was designed for off-line use primarily as a benchmark for evaluating various non- or suboptimum trajectories. Various simplifications are possible to reduce the computer complexity for onboard implementation. For example, the iteration loop to achieve a specified range need not be mechanized. This approach was used in a piloted simulation of the algorithm (Ref. 9). In that study, the pilot played an active part in closing the loop on range.

RESULTS

The computer-implemented version of this algorithm was used to compute and to study the characteristics of several types of optimum trajectories. This section presents a summary of the results. A more complete discussion, including the effects of winds, nonstandard temperatures, and gross weight changes, can be found in Ref. 8. The aerodynamic and propulsion models used in these calculations are representatives of the Boeing 727-100 aircraft equipped with JT8D-7A engines. The time and fuel cost parameters in the performance function Eq. (7) were chosen to be \$500/hr and 6.23 cents/lb, respectively. Inflation has increased these

parameters since their selection in early 1978. However, because the trajectories actually depend only on the ratio of the parameters, the trajectories continue to be useful, especially for comparing minimum fuel and DOC cases.

Figure 10(a) shows the altitude vs range for 100, 200, and 1000 n. mi. range minimum DOC trajectories. The aircraft takeoff weight for these trajectories is 150,000 lb. Winds are assumed to be zero and atmospheric conditions are for a standard day. For the 200-n. mi. range, both the constrained thrust (solid line) and the free thrust (dashed line) trajectories are shown. Also, for the 200-n.mi. range, Fig. 10(b) shows the corresponding altitude vs airspeed profiles.

Below 10,000 ft altitude, all trajectories are essentially identical in both climb and descent profiles. At 10,000 ft both the climb and descent profiles are interrupted by short segments of almost level flight. These are the result of the 250 KIAS speed limit imposed on the trajectory below 10,000 ft by U.S. air traffic control rules. Thus, when the aircraft reaches 10,000 ft in climb, the aircraft accelerates to the unconstrained optimum climb speed (see Fig. 12(b)). Similarly, a deceleration occurs in descent at this altitude.

The constrained thrust trajectories for the 100- and 200-n. mi. ranges contain short cruise segments below the optimum cruise altitude of 31,000 ft. Optimal cruise altitude is used for ranges longer than about 250 n. mi. For the relatively long range flight of 1000 n. mi., the optimum cruise altitude increases at a rate of approximately 2.5 ft/n. mi. of cruise distance due to fuel burnoff.

The free thrust trajectory for the 200-n. mi. range does not contain a cruise segment. However, the difference between the constrained and free thrust profiles is slight and is noticeable only above 25,000 ft. Below this altitude the optimum thrust values are identical for both types, namely, maximum in climb and idle in descent. Above this altitude the thrust reduces gradually in climb for the free thrust case; it continues to reduce during the initial descent and reaches idle thrust at 20,000 ft. Differences in the speed profiles also are noticeable only above about 24,000 ft. As expected, the difference in operating costs between the two types of trajectories is slight, amounting to an additional $8 saving for the 200-n. mi. free thrust trajectory.

Minimum fuel trajectories, obtained by setting the time cost parameter in the performance function to zero, are shown in Fig. 13. In comparison with the minimum DOC trajectories, the minimum fuel trajectories for a given range climb to a higher altitude and use a substantially lower airspeed above 10,000 ft. Also, above 10,000 ft the flight-path angle of the minimum fuel trajectories is steeper in climb and shallower in descent. As before, differences in the altitude profiles between the constrained and unconstrained thrust trajectories are apparent only near the top of the climb. The penalty in fuel consumption due to the 250 KIAS speed restriction below 10,000 ft was found to be 66 lb. This penalty increases with an increase in gross weight but is essentially independent of range.

Table 1 summarizes several important numerical values for the trajectories calculated. Comparison of tabulated figures shows that the fuel saved by flying the minimum fuel instead of the minimum DOC trajectory is about 1,000 lb for the 1,000-n. mi. range, or about 1 lb/n. mi. However, the associated time and cost penalties are 16 min and $80, respectively. If the price of fuel continues to increase more rapidly than the cost of time, as was the case in 1979, the optimum DOC and fuel trajectories will converge, resulting in smaller fuel and cost differences between them.

For the 200-n. mi.-range minimum fuel trajectories, the differences in fuel consumption between the constrained and free thrust cases is 23 lb. This relatively small difference would seem to justify the use of the simpler-to-mechanize and computationally faster constrained thrust mode, especially in an onboard computer implementation. However, as was pointed out in the preceding theory sections, this difference is aircraft- and propulsion-model dependent and therefore should be checked whenever there is a change in model characteristics.

CONCLUSIONS

The approach presented here has established the structure of optimum trajectories for airline operations and has yielded an efficient computer algorithm for calculating them. The algorithm can be incorporated in an airline flight planning system or can be used to determine the performance penalty of simplified onboard algorithms. The latter application is important at this time in view of the current effort by industry to develop onboard performance management systems.

Two pairs of opposing assumptions, constrained vs free thrust and dependence vs independence of specific fuel consumption on thrust, played pivotal roles in determining the characteristics of the optimum trajectories. If the assumption of specific fuel consumption independent of thrust is justified, constrained thrust trajectories are identical in structure and performance to free thrust trajectories. However, when the realistic dependence of specific fuel consumption on thrust is taken into account, there will be a difference, though slight for the example studied, in both performance and structure between constrained and free thrust cases. The actual differences in performance depend on the propulsion and aerodynamic models as well as other factors and must be determined for each aircraft model by computer calculation.

APPENDIX

It is to be proved that the loci of $\dot{W}_f - \lambda V = 0$ and $T - D = 0$ are tangent at the cruise point, assuming that the cruise point at $T = T_C$, $V = V_C$ is a minimum of the cruise cost $\dot{W}_f/V$ along the locus $T - D = 0$. This is equivalent to proving that the cruise point lies on both loci and that the slopes of the loci are identical at that point.

That the cruise point satisfies $\dot{W}_f - \lambda V = 0$ follows from the sequence of relations below:

$$(\dot{W}_f - \lambda V)\Big]_{\substack{T=T_c \\ V=V_c}} = V\left(\frac{\dot{W}_f}{V} - \lambda\right)\Big]_{\substack{T=T_c \\ V=V_c}} = V_c\left\{\left(\frac{\dot{W}_f}{V}\right)\Big]_{\substack{T=T_c \\ V=V_c}} - \lambda\right\} = V_c(\lambda - \lambda) = 0$$

To prove that the slopes are identical, compute the gradient of $\dot{W}_f - \lambda V$:

$$\nabla(\dot{W}_f - \lambda V) = \hat{i}\left[TS_{FC_V} - \frac{TS_{FC}}{V}\right]_{\substack{T=T_c \\ V=V_c}} + \hat{j}\left[TS_{FC_T} + S_{FC}\right]_{\substack{T=T_c \\ V=V_c}} \tag{A1}$$

The perpendicular unit vectors $\hat{i}$ and $\hat{j}$ point in the speed and thrust directions, respectively. Now write λ as a function of the perturbation ΔV:

$$\lambda = [(T_c + D_V\,\Delta V)S_{FC}(T_c + D_V\,\Delta V,\ V_c + \Delta V)]/(V_c + \Delta V) \tag{A2}$$

Since, by assumption, λ has a minimum at $V = V_c$, set the derivative of λ with respect to ΔV equal to zero. This yields the following relation:

$$\lambda = D_V S_{FC} + T_c\left(S_{FC_T} D_V + S_{FC_V}\right) = T_c S_{FC}/V_c \tag{A3}$$

Next compute the gradient of $(T - D)(V/W)$ at the cruise point:

$$\nabla(T - D)(V/W)\Big]_{\substack{T=T_c \\ V=V_c}} = (V_c/W)[\hat{i}(-D_V) + \hat{j}] \tag{A4}$$

The slope of Eq. (A1) relative to the $\hat{i}$ direction is given by

$$\text{Slope} = \frac{\left(T_c S_{FC_V} + S_{FC}\right)}{\left[T_c S_{FC_V} - (T_c S_{FC}/V_c)\right]} \tag{A5}$$

After substituting Eq. (A3) in place of $T_c S_{FC}/V_c$ in Eq. (A5), the slope simplifies to $-1/D_V$, which is identical to the slope of Eq. (A4).

REFERENCES

1. Erzberger, H., McLean, J. D., Barman, J. F.: Fixed-Range Optimum Trajectories for Short Haul Aircraft. NASA TN D-8115, Dec. 1975.

2. Speyer, J. L.: Nonoptimality of the Steady-State Cruise for Aircraft. AIAA J., Vol. 14, Nov. 1976, pp. 1604-1610.

3. Barman, J. F., and Erzberger, H.: Fixed Range Optimum Trajectories for Short-Haul Aircraft. J. Aircraft, Vol. 13, Oct. 1976, pp. 748-754.

4. Bryson, A. E., Jr., and Ho., Y-C.: Applied Optimal Control. Blaisdell, Waltham, Mass., 1969, ch. 2.

5. Schultz, R. L., and Zagalsky, N. R.: Aircraft Performance Optimization. J. Aircraft, Vol. 9, Feb. 1972, pp. 108-114.

6. Specific Operating Instructions, JT8D-7 Commercial Turbofan Engines, Pratt and Whitney Aircraft, East Hartford, Connecticut, Jan. 1969.

7. Cooper, L., and Steinberg, D.: Introduction to Methods of Optimization. W. B. Saunders Co., 1970, pp. 147-151.

8. Lee, Homer Q., and Erzberger, Heinz: Algorithm for Fixed Range Optimal Trajectories. NASA TP 1565, Jan. 1980.

9. Bochem. J. H., and Mossman. D.C.: Simulator Evaluation of Optimal Thrust Management/Fuel Conservation Strategies for Airbus Aircraft on Short Haul Routes. Final Report, prepared by Sperry Flight Systems, Phoenix, Ariz. NASA Contractor Report NAS 2-9174, May 1977 - April 1978.

TABLE 1. CHARACTERISTICS OF EXAMPLE OPTIMUM TRAJECTORIES

Thrust mode	Range, n. mi.	Time, hr/min/sec	Cost, $/n. mi.	Fuel, lb/n. mi.	Cruise Altitude/ft	Climb Distance/n. mi.	Descent Distance/n. mi
Minimum Direct Operating Cost Trajectories (150,000 lb Takeoff weight)							
CT[a]	100	20:06	3.58	30.405	14899	43.15	52.66
CT	200	33:02	3.00	25.774	26970	101.42	77.85
FT[b]	200	33:00	2.98	25.331	27827	116.00	84.00
CT	1000	2:13:07	2.28	18.779	30819	135.76	85.38
Minimum Fuel Trajectories (150,000 lb Takeoff weight)							
CT	100	21:26	3.60	29.247	17531	37.73	54.12
CT	200	37:03	3.07	24.38	27226	80.06	83.21
FT	200	37:06	3.06	24.268	28011	101.93	98.07
CT	1000	2:29:14	2.36	17.763	33185	121.07	103.51

[a] CT = Constrained thrust.

[b] FT = Free thrust.

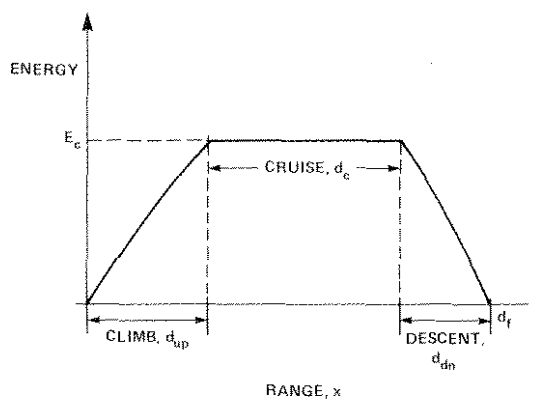

Fig. 1. Assumed structure of optimum trajectories.

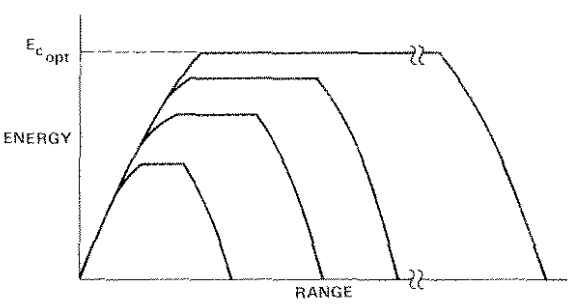

Fig. 3. Energy vs range, H > 0 at E_c.

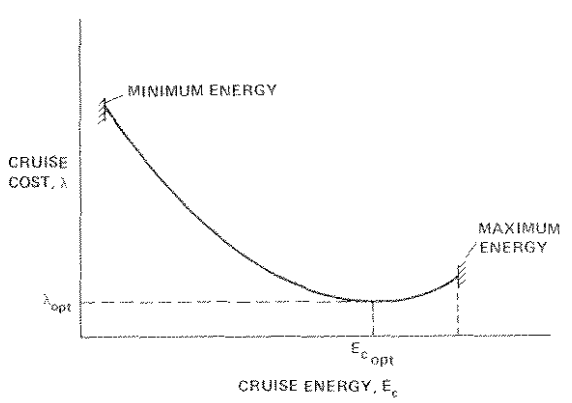

Fig. 2. Cruise cost function.

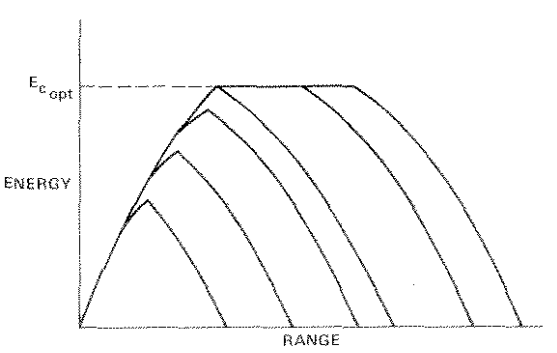

Fig. 4. Energy vs range, H = 0 at E_c.

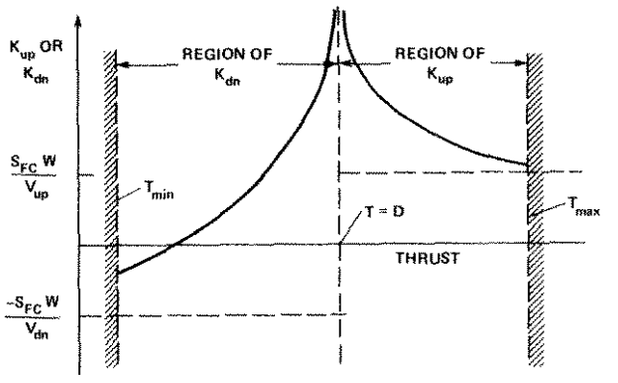

Fig. 5. Illustrating dependence of K_{up} and K_{dn} on thrust.

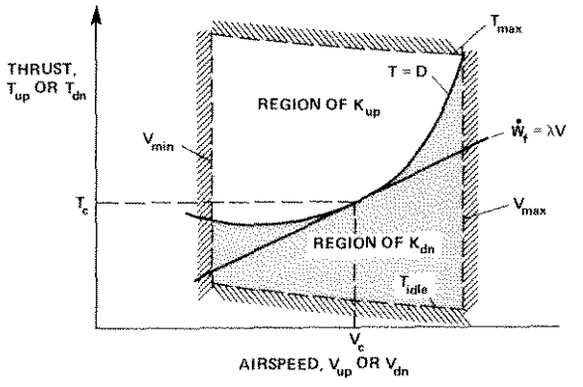

Fig. 6. Loci of T = D and $\dot{W}_f = \lambda V$ in control space at $E = E_c$.

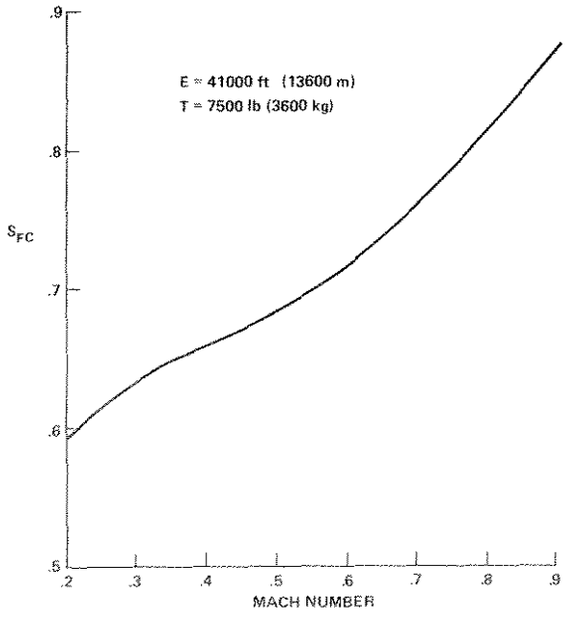

Fig. 7. S_{FC} dependence on Mach Number, JT8D-7.

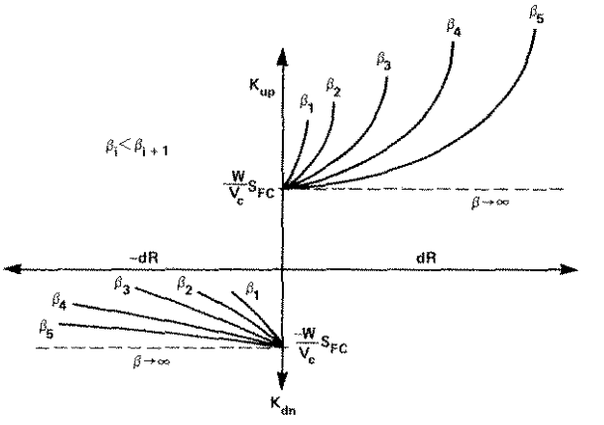

Fig. 8. Dependence of operand function on dR and β at cruise energy E_c.

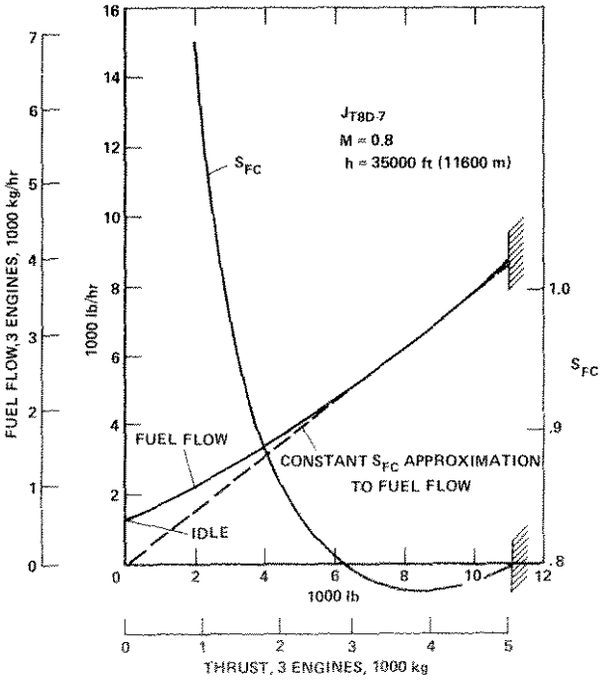

Fig. 9. S_{FC} and fuel flow vs thrust, typical cruise conditions.

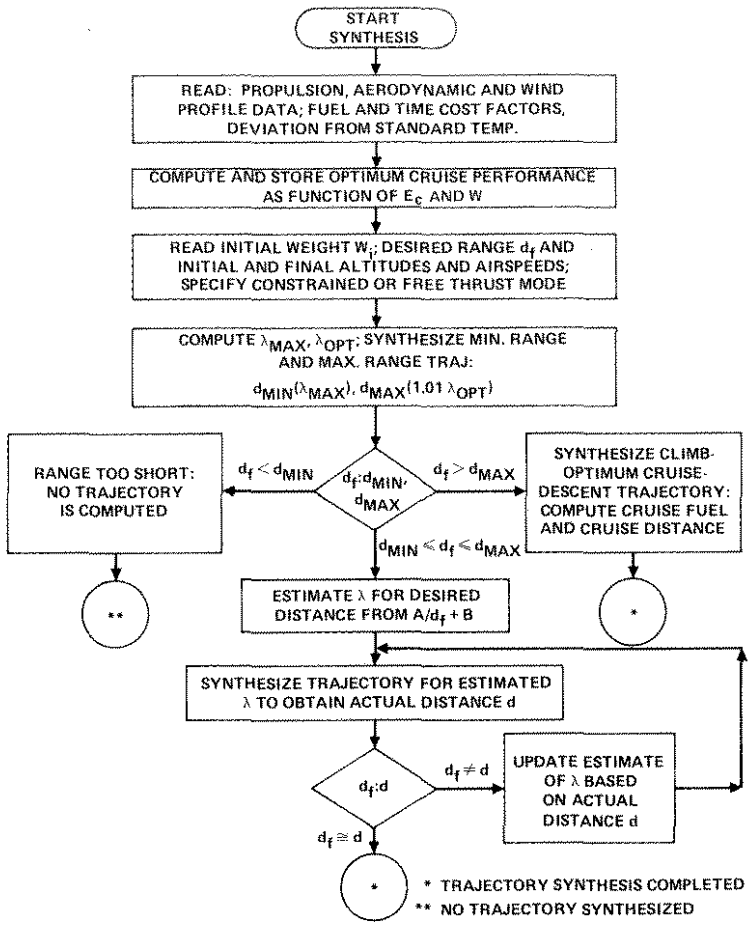

Fig. 10. Flow chart for computer algorithm.

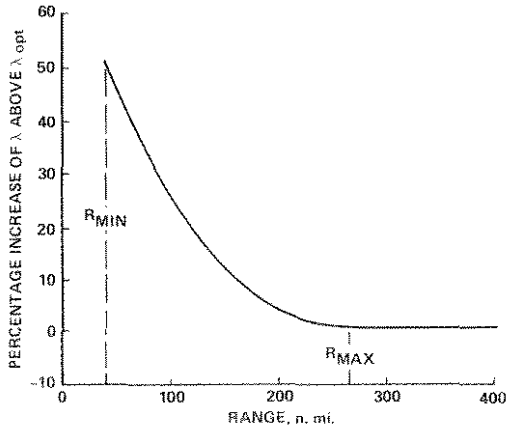

Fig. 11. Typical cruise cost vs range relationship.

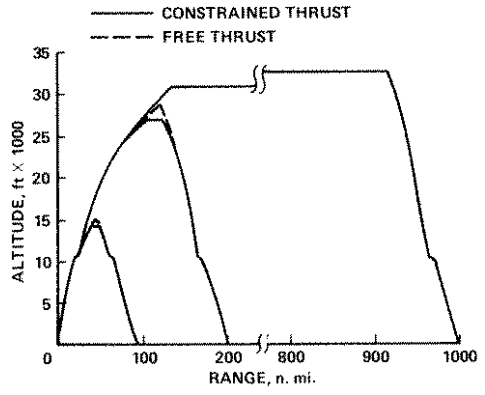

(a) Altitude-range profiles.

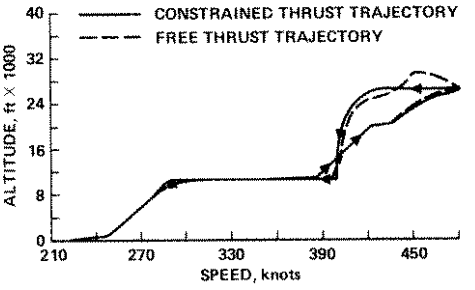

(b) Airspeed-altitude profiles for 200 n.m. range.

Fig. 12. Minimum DOC trajectories.

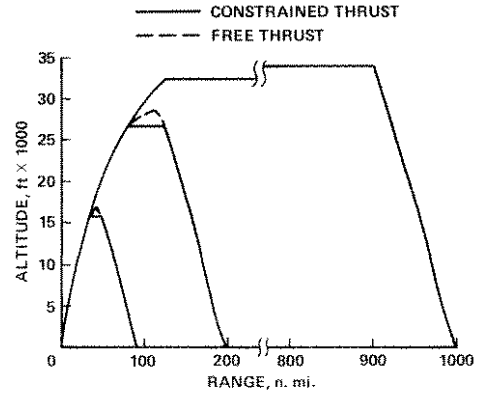

(a) Altitude-range profiles.

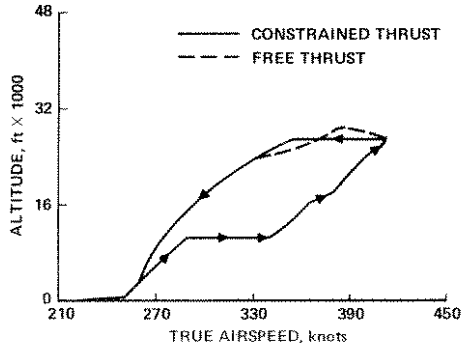

(b) Airspeed-altitude profiles.for 200 n.m. range.

Fig. 13. Minimum fuel trajectories.